Soft Matter

ARTICLE TYPE

Cite this: DOI: 00.0000/xxxxxxxxxx

Electronic Supplementary Information: Deformation-dependent polydimethylsiloxane permeability measured using osmotic microactuators

Alexandra R. Spitzer[a] and Shelby B. Hutchens[a,b,*]

Received Date
Accepted Date

DOI: 00.0000/xxxxxxxxxx

1 Chemical Potential Driven Flux through a Membrane

1.1 Chemical Potential

Chemical potential, μ, is defined as,

$$\mu = \mu_o + RT ln(\chi_l \gamma_l) \tag{1}$$

where μ_o is the reference chemical potential, χ_l is the mole fraction of the solvent, and γ_l is the activity coefficient of the solvent, R is the universal gas constant, and T is the temperature.

1.2 Diffusive Flux Through a Membrane

Flux of the diffusive species water, J_w, is defined as,

$$J_w = -L_w \frac{d\mu_w}{dx} \tag{2}$$

where, L_w is the mobility of the diffusive species water, and $\frac{d\mu_w}{dx}$ is the driving force of water, described by the change in the chemical potential of water across the thickness dimesnion of the membrane, x.

$$J_w \propto \frac{-d\mu_w}{dx} \propto -\frac{\mu_2 - \mu_1}{l} \tag{3}$$

The flux of water across a membrane, is therefore proportional to the chemical potential difference across that membrane. This can be described by the difference of the chemical potentials of solution separated by the membrane, μ_1 and μ_2, which has a thickness of l.

This difference in chemical potential on either side of the membrane and resulting non-equilibrium condition, serves as the driving force for the flux of water across the membrane toward chemical equilibrium between solutions separated by the membrane.

To understand the difference in chemical potential between the encapsulated salt solution and pure water reservoir, the chemical potentials of each of the individual solutions must be defined. For low solute concentrations, the activity coefficient of water, γ_w, is approximately 1. Here $\chi_{w,pure}$ describes the mole fraction of pure water, and $\chi_{\text{w,salt solution}}$ describes the mole fraction of the water in the salt solution.

$$\mu_{\text{w,pure}} = \mu_{\text{o,water}} + RT \ln(\chi_{\text{w,pure}}) \tag{4}$$

$$\mu_{\text{w,salt solution}} = \mu_{\text{o,water}} + RT \ln(\chi_{\text{w,salt solution}}) \tag{5}$$

Subtracting equation 5 from 4, will result in the chemical potential difference between the pure water and salt solution.

$$\mu_{\text{w,pure}} - \mu_{\text{w,salt solution}} = RT \ln(\chi_{\text{w,pure}}) - RT \ln(\chi_{\text{w,salt solution}}) \tag{6}$$

The mole fraction of solvent in pure water is $\chi_{\text{w,pure}} = 1$, so that $RT \ln(1) = 0$. The chemical potential of pure water, $\mu_{\text{w,pure}}$, can alternatively be referred to as the reference chemical potential for water, μ_o, and therefore we denote $\mu_{\text{w,salt solution}}$, as μ. Combining these statements with equation 6 results in:

$$\mu = \mu_o + RT \ln(\chi_{\text{w,salt solution}}) \tag{7}$$

For a solution with a low solute mole fraction, χ_{salt}, the mole fraction of solvent, $\chi_{\text{w,salt solution}}$, is relatively high. This solvent mole fraction can alternatively be expressed as $1 - \chi_{\text{salt}}$.

$$\mu = \mu_o + RT \ln(1 - \chi_{\text{salt}}) \tag{8}$$

For small values of χ_{salt}, a Taylor series expansion can be used, yielding

$$\mu = \mu_o + RT \ln(-\chi_{\text{salt}}) \tag{9}$$

This salt mole fraction can be expressed as the ratio of moles of salt present, n_{salt}, to the total moles present in solution, $n_{\text{salt}} +$

[a] Department of Materials Science and Engineering, University of Illinois Urbana-Champaign, Urbana, IL, USA.
[b] Department of Mechanical Science and Engineering, University of Illinois Urbana-Champaign, Urbana, IL, USA. E-mail: hutchs@illinois.edu; Tel: +1 (217)300-0412

n_{water}.

$$\mu = \mu_o + RT \ln\left(-\frac{n_{\text{salt}}}{n_{\text{salt}} + n_{\text{water}}}\right) \tag{10}$$

The osmotic potential of a solution, as defined by Van't Hoff, describes the pressure necessary to keep solvent from flowing into a a concentrated region,

$$\Pi = -i\frac{n_{\text{salt}}}{V}RT, \tag{11}$$

where i is the electronic dissociation factor of the ionic solute.

Combing equations 10 and 11, results in the following expression relating the chemical potential to the osmotic potential and and solution properties, where $V_m = \frac{V}{n_{\text{water}}}$ and describes the molar volume of water .

$$\mu = \mu_o + \frac{\Pi V}{n_{water}} = \mu_0 + \Pi V_m \tag{12}$$

The reference chemical potential depends on the systems' pressure, $P = P_{atm} + P_t$. Here P_{atm} describes the atmospheric pressure, and P_t describes the turgor pressure or hydrostatic pressure on one or both sides of a membrane. Understanding this dependence, Equation 12, can be written to explicitly indicate pressure terms,

$$\mu = \mu_0(P_{atm} + P_t) + \Pi V_m. \tag{13}$$

At a constant temperature, Gibb's free energy is defined as, $d\mu = VdP - SdT$. We assume constant temperature and constant atmospheric pressure, allowing for the re-expression of 13 as,

$$\mu = \mu_0(P_{atm}) + \Pi V_m + \int_{P_{atm}}^{P_{atm}+P_t} V_m(P)dP \tag{14}$$

For an incompressible substance, which is a reasonable approximation for water over the range of pressures we attain, this integral reduces to $V_m P_t$, resulting in,

$$\mu = \mu_0(P_{atm}) + \Pi V_m + V_m P_t \tag{15}$$

This can rearranged to form the expression,

$$\mu - \mu_0 = V_m(P_t + \Pi) \tag{16}$$

Combining Equations 2 and 16, results in a pressure dependent equation for diffusive flux of species i through a membrane, which is expressed in units of $\frac{mol}{m^2 s}$.

$$J_w = \frac{-L_w V_m}{l}(\Pi + P_t) \tag{17}$$

1.3 Diffusive Flux and Diffusivity Relationship

When discussing permeability and diffusion of a species, such as water within a membrane, a common term referred to is diffusivity, D_w, which describes the rate at which a species can diffuse through the area of a membrane [$\frac{m^2}{s}$]. Diffusivity is the term that relates the diffusive flux, J_w, to the concentration gradient, $\frac{du_w}{dx}$ that serves as the driving force, as opposed the the chemical potential difference as in the previous section.

$$J_w = -D_w\frac{dC_w}{dx} \tag{18}$$

Diffusivity, D_w, can be related to the mobility, L_w of water within the membrane. From the definition of chemical potential, diffusive flux can be redefined in terms of mole fraction of water, $\chi_w = C_w V$, where C_w is the concentration of water, in volume V.

$$J_w = -L_w RT\frac{dln\chi_w}{dx} = -L_w RT\frac{dln(C_w V)}{dx} = -\frac{L_w RT}{C_w}\frac{dC_w}{dx} \tag{19}$$

This results in the following relationship for mobility in terms of diffusivity,

$$L_w = \frac{D_w C_w}{RT} \tag{20}$$

1.4 Permeability and Diffusivity

In the determination of the rate of flux of a species through a memembrane, two terms are commonly used: diffusivity and permeability. However, these terms are not interchangeable. The diffusivity describes the flux of the water while it is within the membrane, but the permeability encompasses the full membrane, including transport of molecules from the surrounding reservoir into the membrane and transport out of the membrane to the other reservoir. For this reason, in membrane literature, the diffusive flux of water is often described using permeability coefficient prefactor, as follows,

$$J_w = -P_w\frac{dC_w}{dx} \tag{21}$$

In this case, P_w, the permeability coefficient is equal to,

$$P_w = D_w K_{\text{w:membrane}} \tag{22}$$

where D_w is the diffusivity that was described in the previous section, and $K_{w:membrane}$ is known as the sorption or partition coefficient of water and the membrane. Here, the sorption describes the ratio of concentrations of two separate components in in the membrane (the membrane matrix, and the diffusive species). In our case, water must dissolve into the membrane from the feed solution, diffuse through the membrane's thickness and then dissolve out of the membrane into the chamber solution. This solubility quantity describes how much water can dissolve into the membrane and will in turn affect the rate of permeation. As we are unable to measure the the content of water in our films, so we can only fit the permeability coefficient. Therefore, we redefine our mobility relationship, using the permeability coefficient, instead of diffusivity, as the rate of diffusion of water through our membrane which also depends on the sorption of water into PDMS.

$$L_w = \frac{P_w C_w}{RT} \tag{23}$$

1.5 Volumetric Flux Through a Membrane

To relate the volume of a species diffusing across a membrane of a given area, we must relate the diffusive flux, J_w, expressed in units [$\frac{\text{mol}}{m^2 \cdot s}$], to a volumetric flux, which we will refer to as J_Q, expressed in units of [$\frac{m^3}{m^2 \cdot s}$]. This can be done by relating the diffusive flux, to the molecular weight of the the solution, M_w,

and the density of the solution ρ.

$$J_Q = \frac{J_w M_W}{\rho} \tag{24}$$

Using this new volumetric flux relationship, we define a volumetric diffusivity for water through our membrane, using the relationships we have described thus far. We combine Equations 17, 20, and24, resulting in,

$$J_Q = -\frac{P_w C_w}{RT}\frac{V_m M_W}{\rho}\frac{(\Pi + P_t)}{l} = -L_w \frac{V_m M_W}{\rho}\frac{(\Pi + P_t)}{l} \tag{25}$$

We define a volumetric mobility, which we denote as L, describing the mobility rate of a volume of water to diffuse through the an area of the membrane per the pressure applied to the membrane. This term is directly related to the permeability coefficient. L is expressed in units $[\frac{m^2}{Pa \cdot s}]$.

$$L = \frac{P_w C_w}{RT}\frac{V_m M_W}{\rho} = L_w \frac{V_m M_W}{\rho} \tag{26}$$

Our new equation expression describing volumetric flux through the membrane, is defined as,

$$J_Q = -\frac{L}{l}(\Pi + P_t) \tag{27}$$

Thus J_Q is expressed in units $[\frac{m^3}{m^2 \cdot s}]$ or $[\frac{m}{s}]$.

2 Ion Diffusion Time Scale for Well-mixed Chamber

We determine that the actuation chambers that we study are well mixed by calculating the time scale for a single sodium ion to diffuse from one side of the chamber to the other. The height of all the chambers is constant with dimensions of $h = 110\ \mu$m. We use this chamber height as the diffusion length scale, determining the time for a single osmolyte ion to travel the from the membrane to chamber floor. This is calculated assuming Fickian diffusion and the Einstein-Smoluchowski Equation:

$$D = \frac{l^2}{2t} \tag{28}$$

where D is the diffusivity of the species, in this case a sodium ion, l is the diffusion length which in this system in the height of the chamber ($h = 110\ \mu$m), and t is the time it takes for this species to diffuse across this length scale. For sodium ions Na^+ the diffusivity in water is $D = 2.098 \times 10^{-9}$ [units:$\frac{m^2}{s}$].[1] Using this information, we solve for $t = 2.88$ s. This short time scale for diffusion across the initial depth of the chamber, leads to our assumption that osmolyte ions in our system can diffuse away from the membrane quickly, meaning that the chamber is well-mixed.

3 Osmotic Pressure Term

The change in osmotic pressure due to the water flow into the chamber is described by the difference in osmotic potential between the chamber and the surrounding feed solution, at a given time.

$$\Delta\Pi(t) = -iRT\left(\frac{n_s}{V(t)} - C_{\text{feed}}\right) \tag{29}$$

The explicit time dependence of this expression can be removed by non-dimensionalizing the volume term by the initial chamber volume V_0, which is the only time dependent term. This nondimensionalized term is the volume ratio of the chamber described by $V(t) = V_0 \frac{V}{V_0}$. At any given instant, the entire volume of the chamber (both the volume under the membrane in addition to the undeformed chamber volume) is described by the non-dimensionalized volume multiplied by the initial chamber volume. The osmotic pressure term can therefore be described by the following expression, removing the time-dependent terms.

$$\Delta\Pi = -iRT\left(\frac{n_s}{(V/V_0)V_0} - C_{\text{feed}}\right) \tag{30}$$

The initial concentration of salt solution encapsulated into the chamber, C_0, is defined as the initial molar quantity of salt in the chamber, n_s, divided by the initial volume of the chamber, V_0. The term $\frac{n_s}{V_0}$ can be replaced by C_0, and factored out of both osmotic pressure terms.

$$\Delta\Pi = -iRTC_0\left(\frac{1}{V/V_0} - \frac{C_{\text{feed}}}{C_0}\right) \tag{31}$$

Finally, as previously discussed the osmotic potential defined by Van't Hoff is $\Pi = -iRTC$, meaning $-iRTC_0$ can be replaced by the initial chamber osmotic potential Π_0. This initial osmotic pressure term can be factored out of the entire expression, to leave an dimensionless osmotic pressure term.

$$\frac{\Delta\Pi}{\Pi_0} = \frac{1}{V/V_0} - \frac{C_{\text{feed}}}{C_0} \tag{32}$$

However, in this system, we utilize a pure water feed solution $C_{\text{feed}} = 0$, meaning $\frac{C_{\text{feed}}}{C_0} = 0$. This leaves the final form of the osmotic pressure term as,

$$\frac{\Delta\Pi}{\Pi_0} = \frac{1}{V/V_0}. \tag{33}$$

4 Linear Elastic Membrane Parameters

We develop a set of membrane bulge parameters to describe the deformation and volume evolution of the system, in terms of linear elastic membrane deformation.

4.0.1 Linear Elastic Surface Area Parameter

Water flow through the selectively permeable membrane results in membrane deformation. The volumetric flow of water is dependent on the surface area of the membrane. This surface area is changing as the membrane is bulging, and therefore we determine the changing surface area with linear elastic behavior, to understand the volume flow rate of water through the membrane. This stretching is time-dependent, and just like previously described, we aim to non-dimensionalize in order to remove the explicit time-dependence. To describe the linear elastic bulging and resulting membrane stretching we use spherical cap geometry relationships. The time-dependent change in this linear elastic membrane is described by the following expression,

$$A(t) = \pi a^2 + \frac{4(V(t) - V_0)^2}{a^4}, \tag{34}$$

where a, is the constant radius of the cylindrical chamber, $V(t)$ is the time dependent volume of the chamber, and V_0 is the initial volume of the chamber at $t = 0$.

The surface area term can be non-dimensionalized by eliminating the time dependence of the volume. This deformation, while explicitly time-dependent is also a function of the membrane bulge volume. For this reason we introduce a dimensionless membrane bulge volume parameter $\tilde{V}$ that quantifies the approximate deflection of the membrane, with respect to the membrane's initial volume V_0, initial area A_0, and chamber radius a, as described by:

$$\tilde{V} = \frac{V(t) - V_0}{A_0 a} = \frac{\frac{V}{V_0} - 1}{\frac{A_0 a}{V_0}} = \frac{\frac{V}{V_0} - 1}{\frac{A_0 a}{V_0}} \tag{35}$$

To nondimensionalize with the membrane deflection parameter we must reconfigure the surface area expression to use the same terms. First, we can nondimensionalize the entire expression, by the initial membrane surface area, $A_0 = \pi a^2$, to determine the normalized change in surface and introduce the A_0 term into the expression. In addition to this we can remove the explicit time-dependence using the same volume ratio term as described previously, $V(t) = V_0 \frac{V}{V_0}$. Employing both of these changes results in the following expression:

$$\frac{A}{A_0} = 1 + \frac{4(\frac{V}{V_0} - 1)^2}{\frac{A_0 a^4}{{V_0}^2}}, \tag{36}$$

This expression can now be related to $\tilde{V}$ the dimensionless membrane deflection term, as $\tilde{V}^2$ can be factored out the expression as follows resulting in a dimensionless membrane surface area expression as a function of $\tilde{V}$.

$$\frac{A(\tilde{V})}{A_0} = 1 + \frac{4A_0\tilde{V}^2}{a^2} \tag{37}$$

4.1 Turgor Pressure Parameter

As water flows through the membrane and the membrane deflects, turgor pressure P_t builds to maintain a static equilibrium. To analytically understand this term with the use of linear elastic mechanics, we follow the assumptions of the Timoshenko theory describing the linear-elastic bulging of a spherical cap[2] as a function of volume change while using the Nix approximation[3]. The increasing volume due to the membrane bulging V_{BM} using this method is described by,

$$V_{BM} = \frac{\pi h}{6}(3a^2 + \delta^2) \approx \frac{\pi a^2 \delta}{2}, \tag{38}$$

where a is the radius of the membrane, δ is the vertical deflection of the membrane center. This Nix approximation holds true for small deflections where $\delta \ll a$. This volume can also be described by subtracting initial chamber volume V_0, from total time-dependent volume of the chamber and added volume under the membrane $V(t)$. This can be nondimensionalized to remove explicit time-dependence using the same nondimensionalization scheme we have utilized previously.

$$V_{BM} = V(t) - V_0 = V_0 \frac{V}{V_0} - V_0 = V_0 \left(\frac{V}{V_0} - 1 \right) \tag{39}$$

In addition to this approximation, we use Timoshenko's linear elastic theory to describe the hydrostatic biaxial pressure in the circular bulging membrane. This can also be referred to as the linear elastic turgor pressure, P_t.

$$p - p_{atm} = P_t = \frac{8 Y l_0 \delta^3}{3a^4}, \tag{40}$$

where Y is the biaxial modulus of the membrane and l_0 is the membrane thickness. The biaxial modulus is related to Young's modulus as $Y = E/(1-\nu)$, and it is assumed that the membrane used is incompressible, meaning $\nu = 0.5$, simplifying the relationship to $Y = 2E$.

The vertical displacement of the bulging membrane at the center δ, can be solved for using Eqns. 38, 39, and expressed as a function of the dimensionless deflection term $\tilde{V}$.

$$\delta = \frac{2V_0(\frac{V}{V_0} - 1)}{\pi a^2} = \frac{2(\frac{V}{V_0} - 1)}{\frac{A_0}{V_0}} = 2\tilde{V}a \tag{41}$$

This new expression for δ is substituted into 40, resulting in the following relationship for turgor pressure as a function of dimensionless stretch term $\tilde{V}$:

$$P_t(\tilde{V}) = \frac{16 E l_0 2\tilde{V} a^3}{3a^4} = \frac{128}{3} \frac{E l_0 \tilde{V}^3}{a}. \tag{42}$$

However, this term still has units of pressure [Pa]. We normalize the entire term the Young's modulus E [units:Pa], resulting in fully a nondimensionlized turgor pressure parameter.

$$\frac{P_t(\tilde{V})}{E} = \frac{128}{3} \frac{l_0 \tilde{V}^3}{a}. \tag{43}$$

5 Hyperelastic Membrane Parameters

We analytically solve for the bulging membrane deformation profile, by parameterizing the undeformed membrane, and solving 5 ODE governing equations that give the solution for the deformed profile as well as the turgor pressure, P_t that causes the deformation. Here we discuss how we utilize the deflection profile solutions to determine hyperelastic membrane deformation parameters utilized in the volume flow rate ODE.

5.1 Non-dimensionalization of membrane geometry parameters

We nondimensionalize all of our geometric membrane parameters for ease of calculation. However, some of the finalized calculations for the stretched membrane constitutive responses rely on quantities with dimensions (surface area, thickness, etc.). Here we define the dimensionless term and their reliance on quantities with dimension, so going forward the two can be converted between with ease.

We non-dimensionalize all initial geometric quantities by the initial radius of the undeformed membrane a, resulting in the

nondimensionalized terms,

$$\tilde{r} = \frac{r}{a}, \qquad \tilde{z} = \frac{z}{a}, \qquad \rho = \frac{\rho'}{a}, \qquad \tilde{\xi} = \frac{\xi}{a}, \tag{44}$$

where the dimensional terms are r (the horizontal coordinate system), z (the vertical coordinate system), ρ' (the initial undeformed parameterized membrane coordinates), and ξ (the membrane arc-length). Therefore, we can further define $\frac{d\rho}{d\rho'} = \frac{1}{a}$, which will aide in further verification of this nondimensionalization method.

With respect to the nondimensionlizing volume, we maintain the same nondimensionalization scheme previously defined for the bulging membrane volume where,

$$\tilde{V} = \frac{V_{\text{deformed bulge}}}{\pi a^3}. \tag{45}$$

To nondimensionalize all the governing equations it is important to check that all stretch ratios with defined with new dimensionless parameters remain dimensionless. First, we verify the longitudinal stretch ratio defined by the change in arc-length ξ over the change in the initial membrane position ρ', can be defined the with the equivalent dimensionless terms ($\tilde{\xi}$,ρ).

$$\lambda_\xi = \frac{d\xi}{d\rho'} = \frac{d(a\tilde{\xi})}{d\rho'} \frac{\frac{1}{a}}{(\frac{d\rho}{d\rho'})} = \frac{d\tilde{\xi}}{d\rho} \tag{46}$$

We verify the latitudinal stretch ratio defined as the r-coordinate over the initial membrane position ρ' is equivalent when defined with $\tilde{r}$ and ρ.

$$\lambda_\phi = \frac{r}{\rho'} = \frac{\tilde{r}a}{\rho a} = \frac{\tilde{r}}{\rho} \tag{47}$$

5.2 Determining the Hyperelastic Bulge Volume

The dimensionless deflection $\tilde{V}$ of the deformed profile is calculated from the device volume gained as a result of the bulging membrane volume, which we input as a boundary condition to solve for the deformed profile. The dimensionless volume is described by the 5th governing equation (Eqn. 48) developed, where $\tilde{V}$ can be found via integration along the $\tilde{z}$ axis for 'disks' of radius $\tilde{r} = \rho\lambda_\phi$.

$$\frac{d\tilde{V}}{d\rho} = \lambda_\phi \rho^2 \frac{d\tilde{z}}{d\rho} \tag{48}$$

5.3 Determining the Hyperelastic Bulging Membrane Surface Area

We determine the dimensionless surface area of each deformed profile $\frac{A}{A_0}$ by integrating over a differential element of length $d\tilde{\xi}(\rho)$ of the deformed membrane from $0 \leq \rho \leq 1$, given by the expression,

$$d\tilde{\xi}(\rho) = \lambda_\xi(\rho) d\rho. \tag{49}$$

This line segment is revolved from $0 \leq \phi \leq 2\pi$ at a radius $\tilde{r} = \lambda_\phi \rho$ about the $\tilde{z}$-axis to obtain an expression for the dimensionless area, $\tilde{A}$. This can be normalized by the initial dimensionless area, $\tilde{A}_0 = \frac{A_0}{a^2}$, yielding,

$$\frac{A}{A_0} = \frac{\tilde{A}}{\tilde{A}_0} = \frac{a^2 \int_0^{2\pi} \int_0^{\tilde{\xi}(1)} d\tilde{\xi} \tilde{r} d\phi}{A_0} = \frac{2\pi a^2 \int_0^1 \lambda_{\tilde{\xi}}(\rho)\lambda_\phi(\rho)\rho \, d\rho}{A_0}. \tag{50}$$

5.4 Determining the Hyperelastic Bulging Membrane's Average Thickness

We calculate the dimensionless inverse average membrane thickness $\langle l_0/l \rangle$ across the entire membrane area by multiplying the expectation value

$$\left\langle \frac{1}{l} \right\rangle = \frac{2\pi a^2 \int_0^1 \frac{1}{l(\rho)} \lambda_\xi(\rho)\lambda_\phi(\rho)\rho \, d\rho}{A} \tag{51}$$

by the initial thickness l_0. Where $l(\rho) = l_0\lambda_r(\rho)$ and invoking incompressibility $\lambda_r\lambda_\xi\lambda_\phi = 1$ gives the final expression

$$\left\langle \frac{l_0}{l} \right\rangle = \frac{2\pi a^2 \int_0^1 (\lambda_\xi(\rho)\lambda_\phi(\rho))^2 \rho \, d\rho}{A} \tag{52}$$

For completeness, we compare the average membrane thickness values $\frac{1}{\langle 1/l \rangle}$ and $\langle l \rangle$ and find that in our case, these quantities are nearly interchangeable. First, we define

$$\langle l \rangle = \frac{2\pi a^2 \int_0^1 l_0\lambda_r\lambda_\xi\lambda_\phi \, d\rho}{A} = \frac{\pi l_0 a^2}{A} = l_0 \frac{A_0}{A}. \tag{53}$$

Fig. S1 plots the inverse of Eqn. 51 and Eqn. 53 as functions of $\tilde{V}$ for the Solaris constitutive parameters and the reference chamber geometry. At greater values of $\tilde{V}$, which corresponds to greater membrane stretching, there is a small deviation between these two approaches to calculating normalized average thicknesses. The normalized average thickness given by $\frac{1}{\langle l_0/l \rangle}$ is predicted to be slightly less than the value predicted by $\frac{1}{l_0/\langle l \rangle}$. We use $\frac{1}{l_0/\langle l \rangle}$ to be more precise.

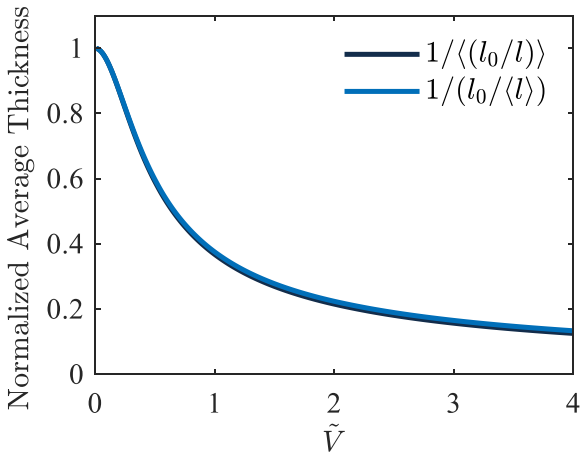

Fig. S1 Normalized average membrane thickness values predicted using two methods ($\frac{1}{\langle l_0/l \rangle}$: dark blue; $\frac{1}{l_0/\langle l \rangle}$: light blue) for bulging actuators as a function of the dimensionless membrane bulge volume $\tilde{V}$. Predicted values are very similar, with a slightly decreased thickness prediction for $\frac{1}{\langle l_0/l \rangle}$, at larger values of $\tilde{V}$ that correspond to greater membrane stretching.

To provide context for the thickness variation across a stretched membrane in comparison to the average membrane thickness (Eqn. (53)), we calculate membrane thickness distribution as shown in Fig. S2. This distribution is provided for an extreme case (standard geometery, highly stretched: $\overline{\lambda}=2.5$, $\tilde{V}=3.5$) and presented as the deviation from the average thickness $l_{\text{average}}=\langle l\rangle$. Under these conditions, there is a variation of $\sim 1\ \mu$m in thickness across the membrane.

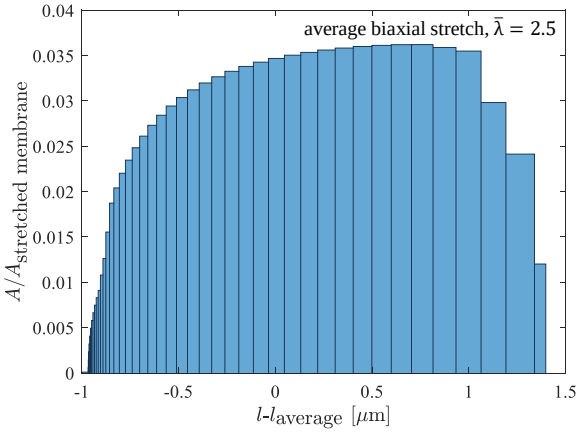

Fig. S2 The distribution of membrane thickness variation relative to the average membrane thickness, $l-l_{\text{average}}$ across the cross sectional area of the membrane. $\overline{\lambda}=2.5$. $\tilde{V}=3.5$. Standard geometry.

5.5 Determining the Hyperelastic Bulging Membrane's Average Biaxial Stretch

We determine the average biaxial stretch in the bulging membrane $\overline{\lambda}$ occurring across the membrane by integrating the biaxial stretch at each discretized ρ value, defined by

$$\lambda(\rho)=\sqrt{\lambda_\xi\lambda_\phi}=\sqrt{\frac{1}{\lambda_r}}, \tag{54}$$

where the average biaxial stretch across the entire membrane, is the expectation value determined by integrating the discretized biaxial stretch about the surface area of the membrane (subsection 5.3),

$$\overline{\lambda}=\langle\overline{\lambda}\rangle=\frac{2\pi a^2\int_0^1\sqrt{\frac{1}{\lambda_r}}\lambda_\xi\lambda_\phi\rho\ d\rho}{A}, \tag{55}$$

divided by the surface area A.

We compare this expectation value average biaxial stretch to an average using the evolution of surface area as given by

$$\overline{\lambda}_{\text{predicted}}=\sqrt{\frac{A}{A_0}}. \tag{56}$$

These two methods, are both plotted in Fig. S3 to compare the average biaxial stretch in the membrane $\overline{\lambda}$, determined using these methods. The expectation stretch quantity $\langle\overline{\lambda}\rangle$, predicts only a slightly increased biaxial stretch at increased membrane bulge volumes of $\tilde{V}\geq 1.5$. Therefore, for simplicity, and since biaxial stretch is provided only for increasing insight, we use $\sqrt{A/A_0}$ to define $\overline{\lambda}$.

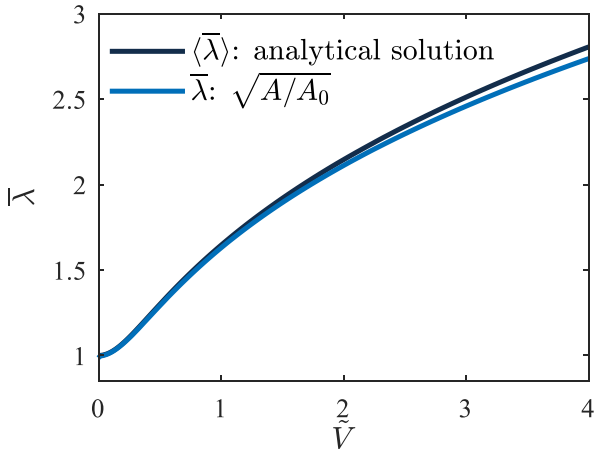

Fig. S3 Average biaxial membrane stretch is predicted using two methods ($\langle\overline{\lambda}\rangle$ (Eqn. 55: dark blue; $\frac{1}{l_0/\langle l\rangle}$ (Eqn. 56): light blue) for bulging actuators as a function of the dimensionless membrane bulge volume $\tilde{V}$. While both of these predictions exhibit similar behavior, $\langle\overline{\lambda}\rangle$ begins to show increased predictions at $\tilde{V}\geq 1.5$.

5.6 Determining Hyperelastic Bulging Membrane Turgor Pressure

Numerically integrating the bulging membrane deformation governing ODEs for a series of given dimensionless volume values $\tilde{V}$, yields a set of solutions, one of which is the applied dimensionless pressure necessary to produce that deformation. The dimensionless turgor pressure $\tilde{P}_t$ is defined as $\tilde{P}_t=\frac{P_t a}{C_1 l_0}$, meaning the turgor pressure with units of [Pa] is $P_t=\frac{\tilde{P}_t C_1 l_0}{a}$. We normalize the applied turgor pressure values by the membrane's Young's Modulus, resulting in $\frac{P_t}{E}$.

5.7 Determining the membrane pre-stretch

Solving this set of hyperelastic governing equations to determine the bulge deformation profile and turgor pressure, requires a set of boundary values, one of which is the initial geometry conditions of the membrane. It was seen throughout the imaging of the actuating chambers, that for all sets of chambers (geometries and materials), that the chambers were expanding slightly at the connection point with the membrane. To accurately capture the deformation profile resulting turgor pressure, we must set the appropriate pre-stretch ratio, $\lambda_{pre}=R(\tilde{V})/R_0$ as the boundary value for the initial membrane radial geometry stretch ratio. This means we set $\lambda_\phi=\lambda_{pre}$ at the membrane edge $\rho=1$. This pre-stretch ratio is determined by using ImageJ to measure the radius of experimentally bulging actuator wells, and fitting a second order polynomial function with an intersection at $R/R_0=1$ to determine the prestretch ratio of chamber as a function of the dimensionless volume $\tilde{V}$. The resulting fit functions for all chamber geometries and materials are shown in Fig.S6.

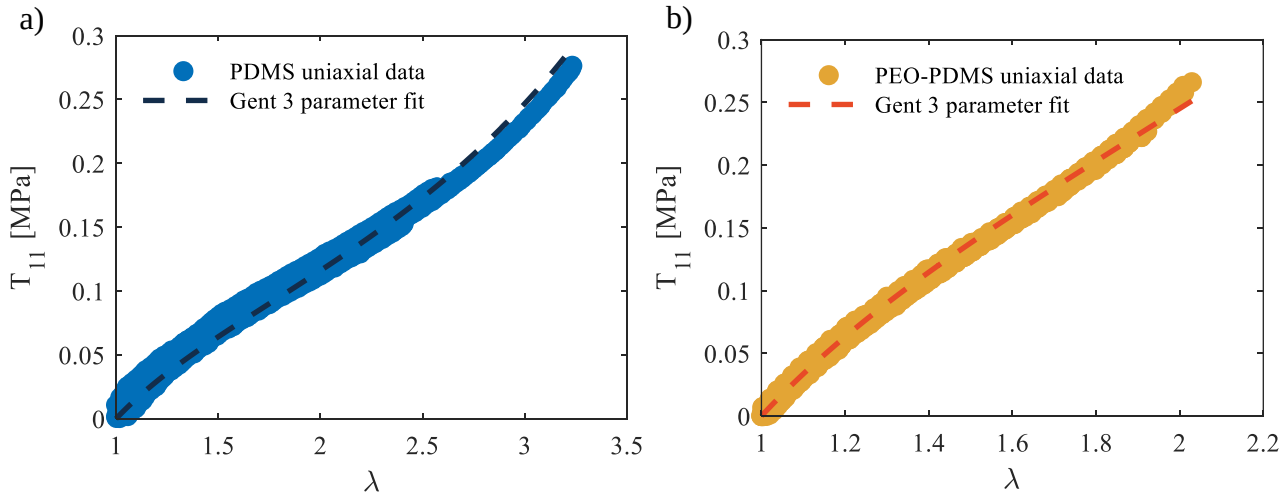

Fig. S4 Mechanical constitutive response behavior for PDMS and PEO-PDMS. (a) Engineering stress T_{11} versus stretch ratio λ for PDMS uniaxial tension test (blue circles), with Gent 3-parameter best fit response plotted (navy dashed line). (b) Engineering stress T_{11} versus stretch ratio λ for uniaxial tension test (gold circles) for PEO-PDMS, with Gent 3-parameter best fit response plotted (orange dashed line).

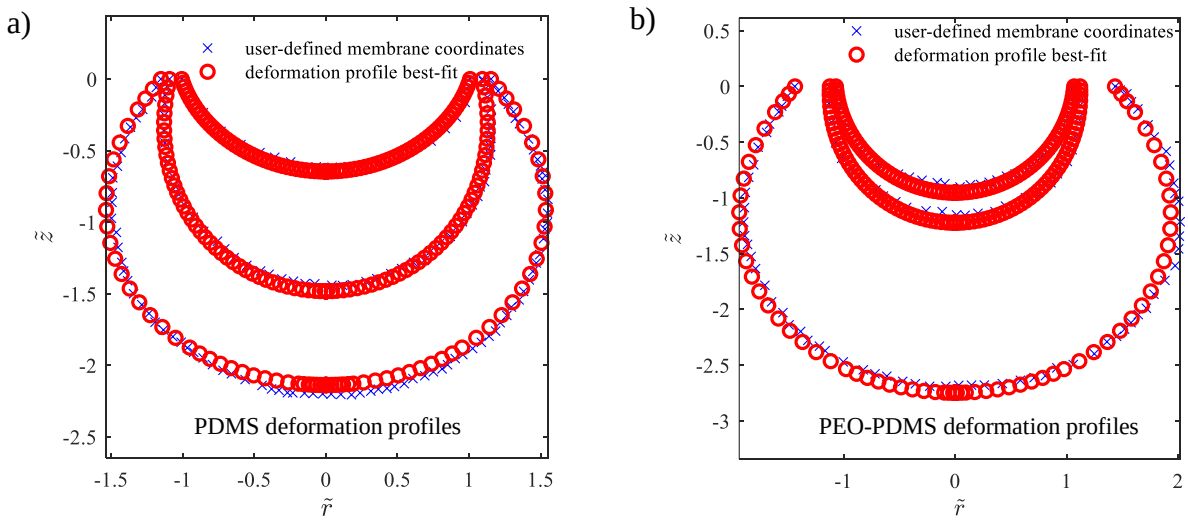

Fig. S5 Mechanical constitutive bulging behavior for PDMS and PEO-PDMS. (a) User-defined deformation profile points for 3 separate bulge volumes (blue x's) and resulting deformation profile best fit (red circles) for PDMS from Gent-3 parameter best fit material parameters. (b) User-defined deformation profile points for 3 separate bulge volumes (blue x's) and resulting deformation profile best fit (red circles) for PEO-PDMS from Gent-3 parameter best fit material parameters.

5.8 Hyperelastic Membrane Mechanics Parameters

The necessary membrane mechanics parameters: $f_A(\tilde{V})$, $f_l(\tilde{V}($, and $f_p(\tilde{V})$ are solved for by individually plotting $\frac{A}{A_0}$, $\frac{l}{l_0}$, and $\frac{P_t}{E}$ on a y-axis against $\tilde{V}$ on the x-axis. Using a spline-fit fit object function in MATLAB to reduce the computational cost of the fit algorithm, a resulting function for each of these three curves were determined per chamber and membrane geometry to solve for the hyperelastic membrane mechanics parameters.

6 Hyperelastic Data Analysis

We use two mechanical test geometries to capture the hyperelastic behavior of PDMS and PEO-PDMS, determining that the Gent 3-parameter model,[4] captures the response of both membrane materials, with different Gent constants for each. This information is used to model the mechanical response and turgor pressure gain of the membranes during deformation. The Gent 3-parameter strain energy density function is as follows,

$$W = -C_1 J_m \ln\left(1 - \frac{J_1}{J_m}\right) + C_2 \ln\left(\frac{J_2+3}{3}\right), \quad (57)$$

with dependence on the first and second strain invariants J_1 and J_2, that are defined as follows,

$$J_1 = \lambda_1^2 + \lambda_2^2 + \frac{1}{\lambda_1 \lambda_2}^2 - 3, \quad (58)$$

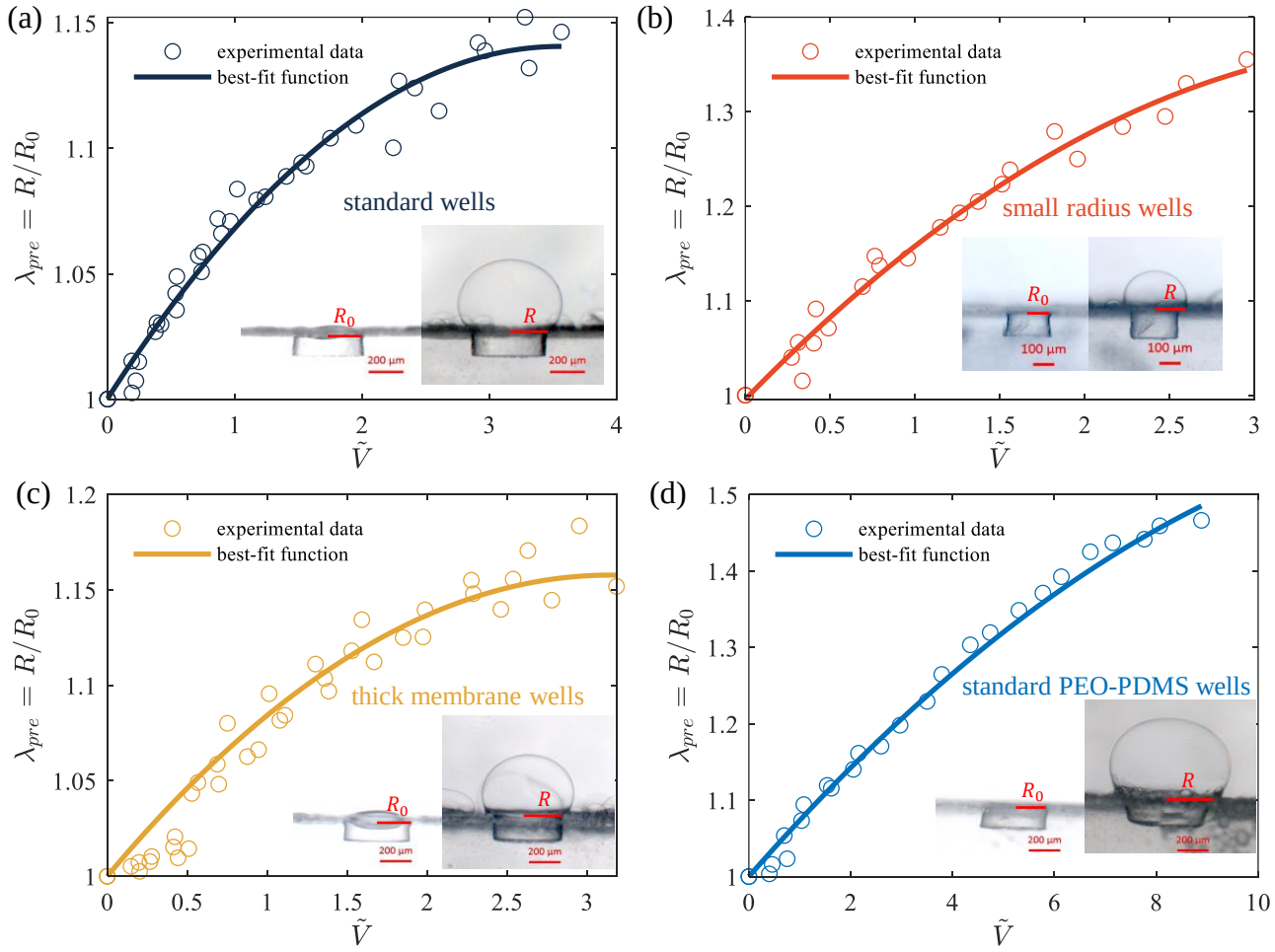

Fig. S6 Radial membrane pre-stretch effect (solid fit line) as a function of deformed bulge volume $\tilde{V}$, determined by fitting a second order polynomial to a set of experimental data (circles) for (a) standard PDMS wells, (b) small radius PDMS wells, (c) thick membrane PDMS wells, and (d) standard geometry PEO-PDMS well.

Table 1 Gent 3-parameter Model Material Constants

Material	C_1 (MPa)	C_2 (MPa)	J_m	E (Young's Modulus) (MPa)
PDMS	0.0316	0.0297	26	0.37
PEO-PDMS	0.0714	0.0536	45	0.75

$$J_2 = \lambda_1^{-2} + \lambda_2^{-2} + \frac{1}{\lambda_1\lambda_2}^{-2} - 3, \tag{59}$$

and assumes incompressibility ($\lambda_1\lambda_2\lambda_3 = 1$), where λ_i is the stretch ratio in each of the three principal directions. Additionally, C_1, C_2 and J_m are materials constants that must be determined by fitting experimentally determined mechanical test data to nominal stress equations derived from this strain-energy density function. C_1 and C_2 are mechanical constants (each with units of [Pa]) that describe the shear modulus G behavior of the material,

$$G = 2(C_1 + C_2). \tag{60}$$

The nominal or engineering stress relation for uniaxial tension, $T_{11,\text{uniaxial}}$, is dependent on the principal stretch ratio along the axis of the applied tension, which is described as $\lambda_1 = \lambda$. Employing the assumption of incompressibility and the uniaxial geometry, the two other principal stretch ratios are given by $\lambda_2 = \lambda_3 = \lambda^{-1/2}$ such that

$$T_{11,\text{uniaxial}} = \frac{1}{\lambda}\left(\frac{C_1 J_m \lambda^2}{J_m - J_1} - \frac{2C_2\lambda^{-2}}{J_2 + 3} - 2(C_1 - \frac{C_2}{3})\right). \tag{61}$$

Simultaneously fitting the uniaxial test data (Fig. S4), and user defined points on three membrane deformation profiles (Fig. S5) to their respective deformation equations derived from Eqn. 57 using nonlinear least square regression in MATLAB, we solve for C_1, C_2 and J_m for both PDMS and PEO-PDMS. The resulting fits are shown in Fig. S4 (the uniaxial response), and Fig. S5 (the fit to user-defined deformation profiles). The material constants are summarized in Table 1. Additionally, we can determine the Young's Modulus E, of each material with these constants using G (Eqn. 60) and the incompressibility assumption,

$$E = 3G. \tag{62}$$

Utilizing the 3 fit parameters as explained above, we find the Young's modulus E, of PDMS and PEO-PDMS are 0.37 MPa and 0.75 MPa, respectively.

7 Determining Bulging Membrane Permeability

We discuss the methods of solving for both stretch-independent and stretch-dependent permeability. Here we provide additional details on these methods and results.

7.1 Constant Linear Elastic Permeability fit

As discussed in the paper, we simultaneously fit experimental PDMS actuation data to the model with linear elastic membrane mechanics parameters, solving for a constant permeability value as the fit parameter. As linear elasticity is only valid for small deflections, we fit this model to actuation data where the biaxial stretch, $\overline{\lambda} \leq 1.4$, which corresponds to volume ratio data $V/V_0 \leq 1.3$. The resulting permeability fit parameter is 2.02×10^{-12} $[\frac{m^2}{s}]$, which is shown in Fig. S7b, and fits the initial small deflection response, but after the linear elastic volume ratio regime, this fit overestimates the response. This permeability value is used to determine the mobility value (Eqn. 26), and then the resulting time constant ($\tau = -\frac{l_0 V_0}{L \Pi_0 A_0}$) for the given chamber configuration that is being used. When the experimental time is nondimensionalized by the chamber's respective time constant τ, the resulting volume ratio actuation behavior collapses in this linear elastic regime for all PDMS chamber configurations, when plotted in dimensionless time $\tilde{t}$, as seen in Fig. S7a.

7.2 Constant Permeability fit

The constant P_w hyperelastic fit discussed in the paper, shows the fit in comparison to the reference chamber conditions ($a = 200$ μm, $l_0 = 20$ μm, $C_0 = 3$ M). Using a nonlinear least-squares regression in MATLAB, we solve for a best-fit permeability of 8.35×10^{-13} $[\frac{m^2}{s}]$. Utilizing this permeability value in our model, the actuation data compared to the theory curve for all PDMS membrane chambers (small radius chamber: $a = 100$ μm, thick membrane chamber: $l_0 = 26$ μm, and reduced osmotic loading: $C_0 = 3$ M) are shown in Fig. S8. This fit parameter captures the middle-time response and high-stretch response behavior of the reference chamber, small radius chamber, thick membrane chamber, and reduced osmotic loading chamber better than the linear fit at large membrane stretch values (later stage actuation). However, it underestimates the initial rate of actuation for these chambers.

7.3 Solving for Stretch Dependent Permeability

We solve for stretch-dependent permeability by isolating the mobility term (and therefore permeability), using the following equation:

$$L(\tilde{V}) = \frac{P_w C_w}{RT} \frac{V_m M_W}{\rho} = -\frac{d\frac{V}{V_0}}{dt} \frac{l_0 V_0}{A_0 \Pi_0} \frac{1}{f_A(\tilde{V}) f_l(\tilde{V})} \frac{1}{\left(\frac{1}{\frac{V}{V_0}} + \frac{E f_p(\tilde{V})}{\Pi_0}\right)} \tag{63}$$

To determine an instantaneous value of mobility L, an instantaneous value of the volumetric flow rate $\frac{dV/V_0}{dt}$ is necessary. We determine a series of instantaneous volume flow rates, by create overlapped time-bins within our data, and using a linear fit function within MATLAB to fit overlapping piece-wise functions to actuation rate data. The resulting slope at each piece-wise linear fit is taken as the instantaneous flow rate $\frac{dV/V_0}{dt}$ at the mid-point time of that binned region. An example of the resulting piecewise fits (dark blue line segments) plotted against the actuation data (dark blue circles) for the reference chamber ($a = 200$ μm, $l_0 = 20$ μm, $C_0 = 3$ M), is shown in Fig. S9.

7.4 Thickness-dependent permeability

As described in the main text, previous studies by Firpo et. al[5] determined a critical length scale L_c at which the surface reactions can become highly nonequilibrium and below which the permeability decreases with decreasing membrane thickness. However, membrane thickness in the deformed state is not uniform, as shown in Fig. S2. To quantify the sensitivity of the thickness dependence to these small thickness changes, we plot the highest and lowest L_c predictions from Fig. 6a, $L_c = 10$ μm and $L_c = 200$ μm, but for a differential membrane thickness, $l - l$, where l is ± 1 μm. Between these differential values, we shade in the regions on Fig. S10 to provide approximate sensitivity analysis of the Firpo thickness-dependence to small thickness changes. The results support our interpretation within the main text.

8 Thin Film Deformation

At high levels of membrane stretching, $\overline{\lambda} = \sqrt{A/A_0} \geq 3.5$, the bulging membranes on the microactuators begin to exhibit color gradients, with the most concentrated color appearing at the maximum deflection in the center of the membrane. Intriguingly, color tends to fall within the blue/violet color spectrum (shown in Fig. S11(a-b)) initially, increasing to warmer colors as the membrane continues to stretch. We hypothesize that these colors appear as the thin film deforms to thicknesses approaching a length-scale close to the wavelength of visible light. Order of magnitude estimations of the film thickness in the region of maximum deflection support this hypothesis (This region has the smallest thickness.) (Fig. S11c).

We obtain film thickness estimates from a combination of experimental observation, finite element calculation, and a few simple geometric relationships. The dimensionless membrane volumes in Fig. S11 (a-b) correspond to $\tilde{V} = 9$ (a) and $\tilde{V} = 10$ (b). We measure the experimental surface area A of these membranes at each of the observed $\tilde{V}$ and estimate the experimental average thickness of these membranes ($l_{\text{exp:average}}$) using the following relationship, assuming incompressibility of the PDMS membrane,

$$l_{\text{average}}(\tilde{V}) = \frac{V_{\text{membrane}}}{A(\tilde{V})} \tag{64}$$

where V_{membrane} is the initial cylindrical membrane volume, defined by a radius of $a = 200$ μm and initial thickness of $l_0 = 20$ μm. The average thickness estimates using this method range from 1.5-1.66 μm, as described in Table 2. In validation,

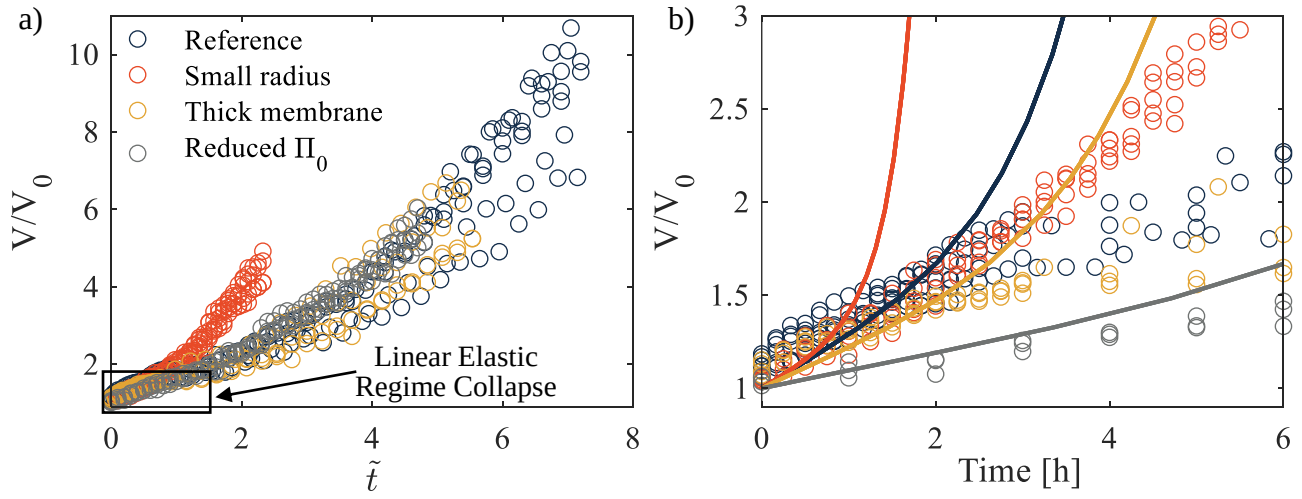

Fig. S7 Linear elastic constant permeability fit. (a) The collapse of all experimental data in the linear elastic regime occurs, when plotted in dimensionless time. (b) The respective best-fit volumetric chamber evolution model employing linear elastic membrane mechanics parameters plotted in experimental time [h], fits each individual experimental chamber configuration, but only in the linear elastic regime ($\frac{V}{V_0} \leq 1.3$).

Table 2 Thin Film Bulging Thickness

$\tilde{V}$	experimental: $l_{\text{average}}(\tilde{V})$ (μm)	prediction: $l_{\text{average}}(\tilde{V})$ (μm)	estimated thickness at max. deflection (nm)
9	1.66	1.34	880
10	1.50	1.23	800

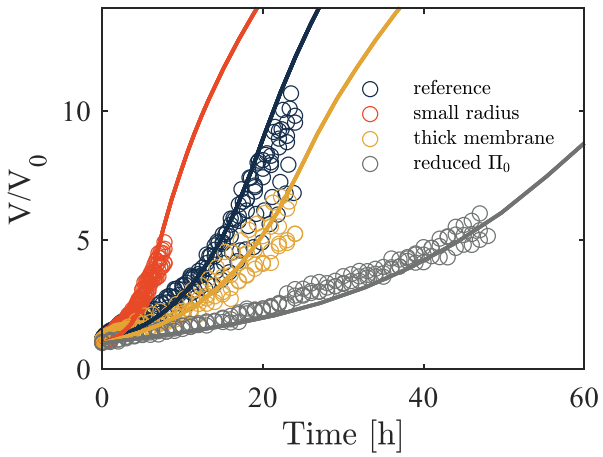

Fig. S8 Constant permeability fit for a hyperelastic membrane shown against experimental actuation. A best fit water permeability P_w is found using nonlinear least-squares regression for all actuation data and utilized in theory to show predictive actuation behavior of a hyperelastic membrane exhibiting constant P_w.

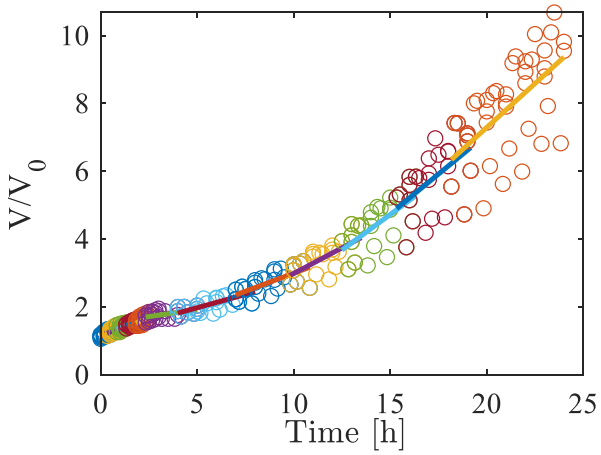

Fig. S9 Piece-wise fits to each small time-binned region of the $\frac{V}{V_0}$ curve, where the slope of each piece-wise linear-function corresponds to the instantaneous volumetric flow rate $\frac{dV/V_0}{dt}$ of each region.

we check these measurements against the average thickness predicted using the constitutive model description of the nonlinear bulge, specifically the inverse of function $f_l(\tilde{V})$. Both values are in agreement as shown in Table 2 with estimates on the same order of magnitude, further demonstrating the consistency of the model in capturing the membrane behavior. Both of these methods (experimental measurement and predictive model) provide average film thicknesses, however the color appearing in the film is concentrated to specific regions, mainly the region at the maximum membrane deflection. This is due to the fact that greater film stretching occurs at the maximum deflection as illustrated by Fig. S11(c). The curves in this figure arise directly from the solutions to the membrane deflection and thickness calculations. Due to incompressibility, the transverse stretch ratio λ_r is the inverse of the product of the longitudinal and latitudinal stretch ratios (λ_ξ, λ_ϕ), and when multiplied by the initial membrane thickness l_0, the stretch dependent membrane thickness along the membrane profile, $l(\rho)$, is defined as

$$l(\rho) = \lambda_r(\rho) l_0. \tag{65}$$

The thickness of the membrane at the membrane's center where

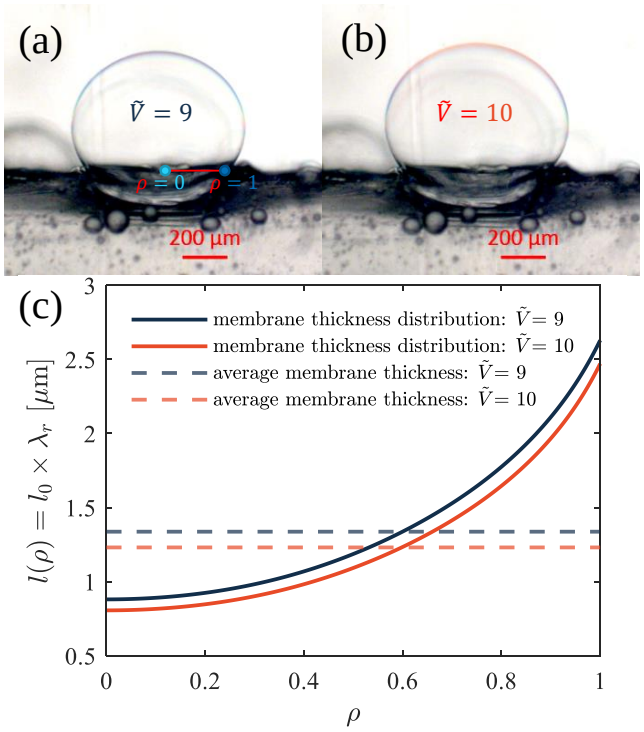

Fig. S11 Thin films deforming on PDMS devices fabricated using the (a-b) reference configuration. At these high levels of deformation [$\tilde{V} = 9$ (a), and $\tilde{V} = 10$ (b)] the bulging membranes begin to exhibit color at the point of maximum deflection. As the membrane experiences greater stretch the color evolves (a: violet color at maximum, b: orange color at maximum). (c) The membrane thickness distribution is non-uniform shown by the solid curves ($\tilde{V} = 9$: blue, $\tilde{V} = 10$: orange), with the thinnest region, occurring at the membrane's center where maximum deflection occurs. This is compared to the average membrane thickness in the entire membrane (dashed line), where the maximum stretch is 34% less than the average stretch.

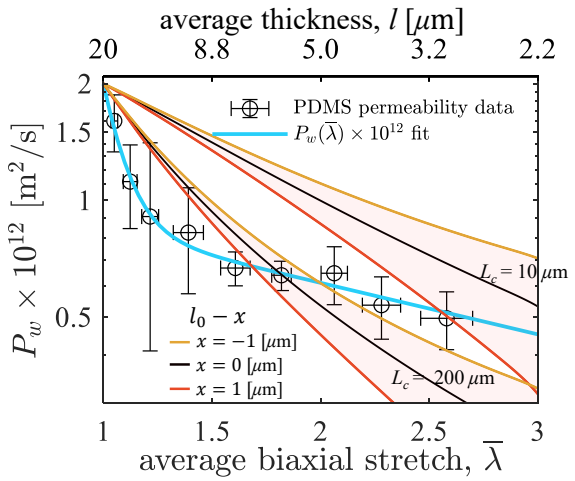

Fig. S10 Deformation-mediated permeability P_w of PDMS where instantaneous permeability (black circles), averaged from all four PDMS chamber conditions, as a function of average biaxial membrane stretch $\overline{\lambda}$ (lower x-axis) and corresponding stretch dependent $P_w(\overline{\lambda})$ fit teal. This permeability-fit is compared to thickness-dependent (l, upper x-axis) permeability model. Shaded regions (light red) bound curves describing L_c at values of (L_c= 10, 200 μm) with $\pm$ 1 μm thickness bounds.

the maximum deflection occurs is at a value of $\rho = 0$. The average membrane thickness is defined by the average thickness $1/\langle l_0/l \rangle$ determined from $f_l(\tilde{V})$, multiplied by the initial membrane thickness l_0

$$l_{\text{average}} = l_0 \frac{1}{\langle l_0/l \rangle}. \tag{66}$$

These average thickness values are plotted in Fig. S11c with dashed lines. The membrane thickness at the center point predict the minimum film thickness (as opposed to using the average film thickness). For both $\tilde{V} = 9$ and $\tilde{V} = 10$, the minimum membrane thickness (which occurs at the maximum deflection) is approximately 34% less than the average membrane thickness. Therefore, the membrane thickness at the maximum deflection (the region where we see concentrated color) for the $\tilde{V} = 9$ and $\tilde{V} = 10$ actuated bulges are approximately 880 nm and 800 nm, respectively. Both values have an order of magnitude similar to that of the wavelength of visible light (400-700 nm).

Notes and references

1 R. Gavara and V. Compan, *JOURNAL OF BIOMEDICAL MATERIALS RESEARCH B: APPLIED BIOMATERIALS*, 2017, **105**, 2218–2231.

2 S. Timoshenko and S. Woinowsky-Krieger, *Theory of plates and shells*, McGraw-Hill, 1959, p. 580.

3 J. J. Vlassak and W. D. Nix, *J. Mater. Res*, 1992, **7**, 3242–3249.

4 A. N. Gent, *International Journal of Non-Linear Mechanics*, 2005, **40**, 165–175.

5 G. Firpo, E. Angeli, L. Repetto and U. Valbusa, *Journal of Membrane Science*, 2015, **481**, 1–8.